



Full Length Article

Atomistic kinetic Monte Carlo simulation on atomic layer deposition of TiN thin film

Sangtae Kim^{a,1}, Hyungmin An^{a,1}, Sangmin Oh^a, Jisu Jung^a, Byungjo Kim^b, Sang Ki Nam^b, Seungwu Han^{a,*}^a Department of Materials Science and Engineering and Research Institute of Advanced Materials, Seoul National University, Seoul 08826, Republic of Korea^b Mechatronics Research, Samsung Electronics Co., Ltd, Gyeonggi-do 18448, Republic of Korea

ARTICLE INFO

Keywords:

Titanium nitride
Atomic layer deposition
Kinetic Monte Carlo simulation
Density functional theory

ABSTRACT

The atomic layer deposition (ALD) process of TiN thin films is widely used in microelectronics, but the detailed growth mechanism is still elusive at the atomistic level. In the present computational study, we carry out kinetic Monte Carlo (kMC) simulations on the ALD process using TiCl_4 and NH_3 precursors. Based on the on-lattice model, we sort out key reactions relevant for the ALD process such as adsorption/desorption of precursors, generation of surface Cl atoms, and evolution of free HCl and Cl_2 molecules. The reaction energies considering local environments are calculated at the level of density functional theory (DFT) while the activation barriers are linearly fitted to sampled cases among distinct reaction families. The resulting kMC model produces the temperature-dependent growth rates and the amounts of Cl residues in reasonable agreement with experiments. The detailed growth pathway is discussed based on the simulation results, which underscores the critical role of surface Cl atoms in the ALD process by generating HCl gas molecules. By revealing the atomistic mechanisms in the TiN-ALD process, the present work would help optimize material properties of TiN thin films.

1. Introduction

Owing to the low electrical resistivity, thermal stability, and chemical inertness, [1] TiN is a key material comprising semiconductor components such as metal gates [2–4], diffusion barriers [5–11], and adhesion/glue layers [12,13]. In growing the TiN thin film, physical vapor deposition (PVD) and chemical vapor deposition (CVD) have been widely used for a long time. PVD enables low-temperature processing, but it suffers from poor step coverage. On the other hand, better step coverage can be obtained by CVD but it requires high-temperature processing above 550 °C to achieve low resistance of the TiN film [14,15]. In addition, CVD introduces byproducts from gas-phase reactions, which contaminates the surface [12,16]. Recently, the atomic layer deposition (ALD) technique became popular in fabricating thin films in microelectronics. In ALD, precursors are alternately introduced to the film surface, separated by the purging step that prevents gas-phase reactions and clears remnant precursors and byproducts. The ALD process of TiN thin films allows for lower-temperature growth than CVD in obtaining desired film qualities, and enables conformal depositions for

structures with high aspect ratios, such as V-NAND or DRAM capacitors.

In the TiN-ALD process, NH_3 is a favored reducing agent while tetrakis(dimethylamino)titanium (TDMAT) and titanium tetrachloride (TiCl_4) are widely selected as metal precursors. Although TDMAT is compatible with low-temperature processing, poor crystallinity and a relatively high resistivity ($> 1000 \mu\Omega\cdot\text{cm}$) due to residual carbon have been reported [17]. Therefore, several works employed the TiCl_4 precursor to attain superior adhesion property and low electrical resistivity ($< 100 \mu\Omega\cdot\text{cm}$) [18–20]. However, the density of Cl impurities rises at low temperatures, increasing the resistivity [19,21,22]. To suppress Cl impurities, additional co-reactants such as Zn [22,23], AlMe_3 [24,25], and H_2S [26] have been introduced.

In spite of the wide use in microelectronic devices and extensive studies on surface chemistry, the fundamental understanding of TiN-ALD processes employing TiCl_4 and NH_3 is far from being satisfactory. For instance, even the basic reaction formula is still elusive; because of imbalance in the number of Cl and H ligands in the precursors, gas molecules other than HCl are necessary to satisfy 1:1 stoichiometry of TiN. While the generation of N_2 molecules is thermodynamically

* Corresponding author.

E-mail address: hansw@snu.ac.kr (S. Han).¹ These authors contributed equally.

favorable and also widely acknowledged in the CVD process [14,27], N₂ molecules were not detected in the mass spectroscopy during ALD [24]. From the XPS study, it was suggested that Cl₂ molecules can be formed through the dissociation of TiCl₄ although the process is thermodynamically unfavorable [28]. In addition, it is unclear how the Cl impurities are incorporated into the film (see above), which hampers further optimization of the growth process.

The above discussion calls for further understanding of the reaction mechanism in TiN-ALD processes, in particular at the atomistic level. The experimental analysis is limited in probing surface reactions with full atomistic details, which can be complemented by the computational simulation. Since the ALD process consists of surface reactions with significant activation barriers, *ab initio* molecular dynamics (MD) simulations are not suitable for investigating the whole ALD process because most of the simulation time will be spent on local vibrations. By coarse-graining atomic vibrations and focusing on reaction events, the kinetic Monte Carlo (kMC) method can simulate the experimental time scale [29,30]. Thus, to explore the reaction chemistry of TiN-ALD at the atomic scale, we herein carry out an atomistic kMC simulation parameterized by the density functional theory (DFT) calculations. The kMC method has been applied to ALD simulations for the growth of Al₂O₃ [31], HfO₂ [32,33], ZnO [34], and MgF₂ [35]. While previous DFT studies addressed reaction paths in TiN CVD [36–38] or the initial stage of TiN-ALD [39], there has been no kMC study on the TiN-ALD process as far as we are aware. Based on kMC simulations, we explore thermodynamics and kinetics of surface reactions that play key roles in the ALD growth of TiN. The rest of the paper is organized as follows: in Sec. 2, we briefly introduce the computational approach and discuss on the model system and chemical reactions that are considered in the kMC simulation. The computational results are presented and discussed in Sec. 3. Finally, we summarize the main results in Sec. 4.

2. Methods

2.1. KMC simulation

Below, we briefly explain the kMC method. For the full details, we refer to a recent review article [29]. In kMC, the simulation focuses on the transition between local minima, where small vibrations are coarse-grained, and assumes a history-independent probabilistic network process (Markov-chain process). In principle, one can explicitly solve the Markovian master equation:

$$\frac{dP_i(t)}{dt} = \sum_{j \neq i} k_{ji} P_j(t) - \sum_{j \neq i} k_{ij} P_i(t), \quad (1)$$

where $P_i(t)$ means the probability of the system being in the state i at time t , and k_{ij} indicates the rate constant for the transition from state i to j . Since this coupled equation is hard to solve except for a few cases [40], in kMC one constructs the trajectory of state-to-state transition in a stochastic way. Among several algorithms to achieve this strategy, the Bortz-Kalos-Lebowitz (BKL) algorithm is highly favored [41]. In the BKL algorithm, one first enumerates all the possible transitions or events (N in total) for the given state, together with associated rate constants (k_i). Then the total rate constant (k_{tot}) is obtained by adding all the individual rate constants:

$$k_{\text{tot}} = \sum_{i=1}^N k_i, \quad (2)$$

where i indicates a particular event. A random number, $\rho_1 \in (0,1]$ is generated and used to select an event j satisfying:

$$\sum_{i=1}^{j-1} k_i < \rho_1 k_{\text{tot}} \leq \sum_{i=1}^j k_i. \quad (3)$$

After the selected event is executed, the present state is updated

accordingly. Finally, the simulation time is advanced by Δt defined in the following:

$$\Delta t = -\frac{\ln(\rho_2)}{k_{\text{tot}}}, \quad (4)$$

where ρ_2 is a random number $\in (0,1]$. The time advance is independent of the rate constant of the chosen event but does depend on the total sum of rate constants (k_{tot}). This means that when fast events (i.e., events with large rate constants) dominate the event list, the system clock advances slowly.

For the thermally activated process, the rate constant (k_{ij}) can be calculated within the transition-state theory (TST) using the Eyring equation [42]:

$$k_{ij} = \frac{q_{\text{TS}}^{\text{vib}}}{q_i^{\text{vib}}} \frac{k_{\text{B}} T}{h} \exp\left(-\frac{E_{ij}^{\ddagger}}{k_{\text{B}} T}\right) = k_0 \frac{k_{\text{B}} T}{h} \exp\left(-\frac{E_{ij}^{\ddagger}}{k_{\text{B}} T}\right), \quad (5)$$

where $q_{\text{TS}}^{\text{vib}}$ and q_i^{vib} are the vibrational partition functions at the transition state (TS) and the initial state i , respectively, with k_0 the ratio between them, k_{B} the Boltzmann constant, T the temperature, h the Planck constant, and E_{ij}^{\ddagger} the activation barrier. While one can calculate the pre-exponential factor k_0 from the normal mode analysis of the initial and transition states, it is usually assumed to a value between 1 and 10 [29], and we set $k_0 = 1$ in the present work.

The adsorption of gas molecules such as TiCl₄ and NH₃ is a non-activated process, and the rate constant (k_{ads}) can be obtained by the kinetic gas theory [43]:

$$k_{\text{ads}} = \frac{P\sigma(T, \theta)}{\sqrt{2\pi m k_{\text{B}} T}} A, \quad (6)$$

where P is the partial pressure of gas, σ the sticking coefficient that depends on the temperature T and surface coverage θ , m the molecular mass of the species, and A is the active area. In the present work, A is approximated as the total area of the TiN surface divided by the number of reactive sites in the simulation cell, and the sticking coefficient σ is set to unity regardless of T and θ to make adsorption always occur. On the other hand, the desorption process is regarded as a chemical reaction that breaks bonds with the surface and escapes as a gas molecule. As with thermally activated processes, the desorption rate is calculated within TST in Eq. (5) and the absolute value of adsorption energy serves as the activation barrier of desorption.

2.2. Lattice model

The present lattice model is based on the rock salt structure of TiN. During the ALD process, [200] and [111]-oriented planes coexist as polycrystals depending on the process temperature and substrate condition [19,20,26,44,58]. Generally, (111) surface is major at high temperatures, except for Ref. [19] that reported a 1:1.3 ratio of (111) and (200) surfaces. At low temperatures, (200) surface is major, except for Ref. [44] where the (111) surface was major. We choose the (111) plane for the kMC model since it is observed in X-ray diffraction measurements over wide temperature ranges [19,26]. Fig. 1 shows a few layers of the (111) plane of TiN that consists of alternating Ti and N sublattices. The first, second, and third nearest neighbor sites (1NN, 2NN, and 3NN, respectively) with respect to the center site are also indicated.

The species that can occupy the lattice sites encompass precursors (TiCl₄ and NH₃) and various surface species that are produced during the ALD process. Specifically, Ti, TiCl₄, and Cl* can occupy the Ti sublattice while the N sublattice is reserved for N, NH_x ($x = 1, 2, \text{ and } 3$), and Cl. Cl* indicates the Cl atom bonded to NH_x groups after dissociated from Ti (see below). The different occupation rules for the ligand-like Cl and H (i.e., bonded to Ti or N) result from the bond lengths (see precursor models in Fig. 1); the bond length of Ti-Cl is 2.29–2.51 Å, which is comparable to the Ti-N distance of 2.12 Å in the cubic TiN. Therefore,

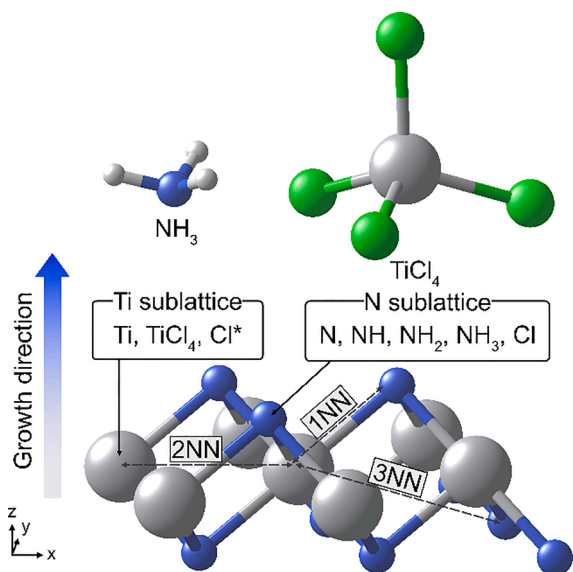


Fig. 1. The ball-and-stick model for the TiN rock salt structure growing in the [1 1 1] crystallographic orientation. 1NN, 2NN, and 3NN neighboring sites with respect to the center site are indicated. The NH_3 and TiCl_4 molecules are also shown at the top.

the Cl atoms are close to the N sublattice when Ti occupies the Ti sublattice. On the other hand, the N-H distance is 1.02–1.03 Å in NH_x , so it is reasonable and convenient to assign NH_x as one species occupying the N sublattice. One exception is that the adsorbed TiCl_4 is assigned to a single site in the Ti sublattice although the molecular size spans multiple sites.

2.3. DFT calculations

Reaction and activation energies are calculated within the density functional theory (DFT) using the Vienna *Ab initio* Simulation Package (VASP) [45–47]. The generalized gradient approximation formulated by Perdew-Burke-Ernzerhof (PBE) [48] is used for the exchange-correlation functional and the DFT-D3 functional [49] is added to describe the van der Waals interactions. The energy cutoff for the plane-wave basis is set to 450 eV, and only the Γ -point is sampled for the Brillouin-zone integration. The base model for DFT calculations is the $12.0 \times 10.4 \text{ \AA}^2$ TiN slab in the (1 1 1) direction. In the case of computing the Cl dissociation (see below), a larger cell of $18.0 \times 10.4 \text{ \AA}^2$ is used to avoid lateral interaction from the periodic boundary conditions. Each layer contains 16 atoms, and two Ti and three N layers are stacked alternately with the surface N layer being mono-hydrogenated (one H atom per N). The surface slabs are separated by a vacuum with the length of 10 Å, and the dipole correction is introduced to remove spurious interactions between periodic slab images. In calculating activation barriers, we employ the climbing-image nudged elastic band (CI-NEB) method implemented in the VASP Transition State Toolkit [50,51]. We use 5 or 7 images along the pathway between initial and final structures. The initial images are generated by image-dependent pair potential method [52] as implemented in the atomic simulation environment code [53]. We ignore the zero-point energy (ZPE) for activation energies. To examine the magnitude of ZPE, we select representative structures from each reaction type and carry out phonon analysis on the initial and transition states. The zero-point corrections are less than 0.1 eV in all the cases, implying that they may not affect the growth behavior significantly.

2.4. Reaction events

In this section, we delineate reaction mechanisms considered within

the present kMC simulation. Exemplary cases for each reaction type are displayed in Fig. 2 as 3-d models as well as 2-d schematic diagrams.

2.4.1. Adsorption and desorption of precursors

TiCl_4 and NH_3 precursors can adsorb at free sites in the Ti and N sublattice by forming bonds with underlying NH_x groups and Ti atoms, respectively. (See Fig. 2a.) The steric hindrance among TiCl_4 molecules constrains TiCl_4 to adsorb on a site whose 2NN Ti sites are all empty. This steric effect consequently limits the maximum coverage of TiCl_4 groups on the surface, which affects the growth rate per ALD cycle. Through HCl evolution or Cl dissociation (see below), the adsorbed TiCl_4 becomes TiCl_3 anchoring to the surface.

2.4.2. Cl dissociation

The Cl ligand around Ti can dissociate and adsorb at the Ti sublattice, which is denoted as Cl^* . (See Fig. 2b.) The Cl^* atoms are significantly stabilized by NH_x groups in the underlying layer owing to the electrostatic interaction with the positively charged H atoms. We find that Cl^* occupying the 1NN site (\times mark in Fig. 2b) is unstable and returns to the original ligand position after structural relaxation. Thus, we posit that Cl^* occupies only 3NN sites. The Cl dissociation allows for dissociative adsorption of TiCl_4 in which one Cl atom dissociates from TiCl_4 and adsorbs to the surface, while the remaining TiCl_3 merges with the surface through strong Ti-N bonds. (See Fig. S1a in the Supplementary information.)

The DFT MD simulations at 300 K show that Cl^* can diffuse rapidly on the surface with low activation barriers, which effectively increases the reaction range of Cl^* . However, if the rapid migration is explicitly simulated within kMC, they would dominate the total rate constant and most computation times would be spent on the diffusion process (called time-disparity problem or stiffness). As an *ad hoc* solution to this, we assume that Cl^* can make an instant jump to 2NN sites (i.e., nearest neighbors in the same plane) before chemical reactions. This effectively increases the range of chemical reactions as will be explained in the below. On a similar note, we prohibit Cl^* from hopping back to the original ligand position.

2.4.3. HCl evolution

The HCl molecule evolves through reaction of H and Cl atoms on the surface. While H originates solely from NH_x groups, there are two types of Cl atoms on the surface: ligand Cl or Cl^* . The ligand Cl horizontally reacts with the adjacent (2NN) NH_x and forms HCl (see ① in Fig. 2c). On the other hand, Cl^* can interact with 1NN NH_x in the lower and upper layers, as indicated by ② and ③, respectively. Because of the layer-by-layer growth, the NH_x groups involved in ② tend to possess higher coordination numbers (CNs) of Ti than those in ③. (The detailed reaction paths can be found in Figs. S1b-d in the Supplementary information.) This gives rise to distinct distributions of reaction and activation energies as will be discussed below. Once the HCl molecule is formed, we assume that it automatically and permanently desorbs from the surface due to a low partial pressure of HCl. This precludes redeposition of HCl molecules to the surface. The adsorbed TiCl_4 can be incorporated into the surface as TiCl_3 after losing one Cl atom through the HCl evolution. In this case, the Cl atom reacts with NH_x in the lower layer.

2.4.4. Cl_2 evolution

Like the HCl evolution, Cl_2 can be formed from two kinds of Cl atoms: Cl or Cl^* . The DFT calculations show that Cl_2 evolutions involving Cl exhibit large reaction energies (> 5 eV) because of relatively weak Cl-Cl bonds compared to Ti-Cl bonds. Therefore, we only consider $\text{Cl}^* + \text{Cl}^* \rightarrow \text{Cl}_2$ as shown in Fig. 2d. This implies that NH_x groups on the surface catalyzes the Cl_2 evolution. Two Cl^* atoms can react when they are in 2NNs, directly or in combination with the instant jump by one Cl^* that reflect the rapid diffusion (see above).

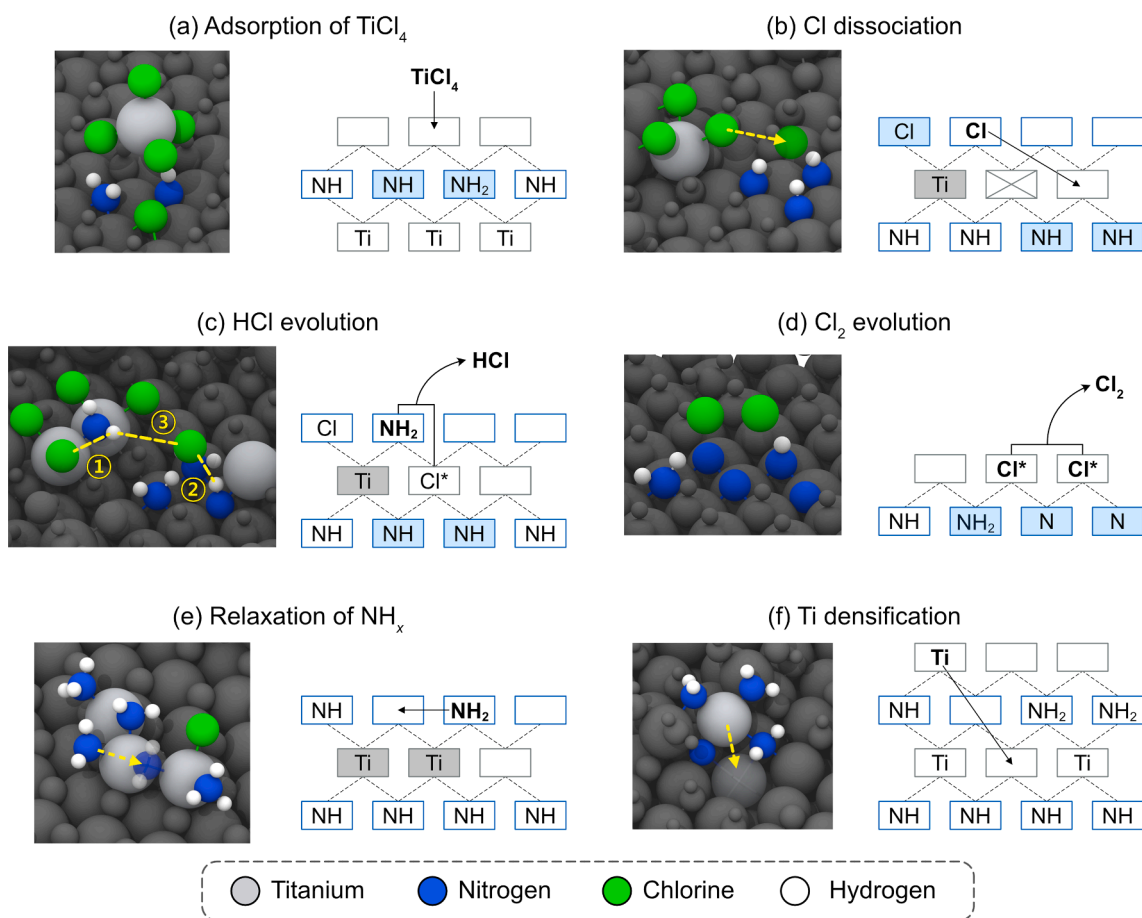


Fig. 2. 3-d model and 2-d schematic diagrams illustrating (a) adsorption of TiCl_4 , (b) Cl dissociation, (c) HCl evolution, (d) Cl_2 evolution, (e) relaxation of NH_x , and (f) Ti densification. In 3-d models, atoms other than reacting species are displayed in dark gray spheres for visual clarity. In 2-d schematics, each box stands for a lattice site in the Ti (gray) or N (blue) layer. Dashed lines between boxes indicate the 1NN relations. Reactions are indicated by arrows and species involved in the reaction are noted in bold symbols. Shaded boxes represent local environments relevant for each reaction.

2.4.5. Relaxation of NH_x and Cl

During the ALD process, local environments around NH_x and Cl can change as a result of chemical reactions, creating more stable sites with higher number of neighboring Ti atoms. In DFT calculations, this leads to spontaneous relaxations of NH_x and Cl in the direction to increase the number of vicinity Ti atoms. To include these reconfigurations within kMC, we assume that NH_x and Cl can move to an adjacent 2NN site if the number of neighboring Ti increases. (See Fig. 2e.) However, if the relaxation requires breaking of the original Ti-Cl or Ti-N bonds, it is excluded because of the significant energy barrier. Since the relaxation is barrierless, we apply a small activation energy of 0.1 eV for this reaction such that the kMC simulation selects the event instantly whenever possible.

2.4.6. Ti densification

During the ALD process, Ti atoms diffuse to sites with higher CNs, which contributes to densification of the thin film (see Fig. 2f). This process also significantly lowers the free energy. The reaction pathway of densification usually involves multi-step collective motions, and it was schematically treated in previous kMC simulations on HfO_2 [33] and ZnO [34] growth. Here we employ a single barrier for Ti densification process. Even though the densification occurs with finite activation barriers, we assume that this process occurs spontaneously with a small barrier of 0.1 eV. We find that the growth rate is rather constant with barriers lower than 1.5 eV, and choose 0.1 eV to ensure that the process occurs whenever possible. Since the strength of Ti-N bonds depends on the coordination number of N, using the low energy barrier

would be realistic at least partly. When the translocated Ti has ligands in the upper layer and those ligands are singly coordinated to the Ti (as shown in the 3-d model), Ti is set to move with the ligands as attached.

Among the key reactions on the surface, we do not consider the hydrogen diffusion among NH_x groups. When we conduct 5-ps MD simulations at 650 K for some cases, we do not find any hydrogen diffusion on the surface, unlike Cl^* diffusion. In sampled cases, the activation energies for H diffusion range over 0.2–1.3 eV. To test the effect of H diffusion within a simplified model, we consider H diffusions with a single barrier of 0.6 eV. The resulting growth rate and Cl contamination at 400 °C change by only 6% and 4%, respectively, with respect to the original model excluding H diffusion. Thus the H diffusion may not be critical in the present ALD simulation.

2.5. Evaluation of reaction and activation energies

Every chemical reaction involves breaking and forming bonds whose strengths are influenced by local chemical environments. In order to consider local environments within reasonable computational resources, we assume that the bond energy is influenced by species occupying 1NN sites around reactants and products whenever applicable. For example, in the Cl_2 evolution in Fig. 2d, initial energies of the two Cl^* atoms depend on NH_x groups at their 1NN sites in the lower layer. There is one exception: in the case of breaking bonds with Ti in NH_3 desorption, Cl dissociation and HCl evolution, we find that strengths of the Ti-Cl or Ti-N bonds are significantly affected by CNs of the Ti atoms. Therefore, we additionally consider the CNs of 1NN Ti

atoms in these reaction types. In Fig. S2, these assumptions on the neighbor influences are validated by computing reaction energies for HCl evolutions with various 2NN configurations.

Even though we tightly constrained the local environments as in the above, there are more than 10,000 possibilities for all the reactions in the previous section, which is a prohibitively large number for DFT calculations. We further reduce the number by imposing symmetry and exclusion rules. For instance, the influence of neighboring species is the same whether the species are bonded clockwise or counter-clockwise. In addition, reactions producing NH or N species bonded to only one Ti atom are energetically unfavorable at relevant temperatures, so they are excluded from the event table. We also find that the reaction energies for the Cl₂ evolution are too high when NH_x groups dominate 1NN sites due to multiple Cl*-H bonds, so such cases are excluded from the Cl₂ evolution.

Table 1 compiles the final number of events for each reaction type counted according to the above conditions, which adds up to ~ 1,200 cases. For the Cl dissociation and HCl evolution, the events are further classified into distinct subtypes. To be specific, Cl dissociation(I) and HCl evolution(I) correspond to dissociative adsorption of TiCl₄ as explained in the previous subsection. (See Fig. S1a for Cl dissociation (I).) Cl dissociation(II) corresponds to the dissociation of Cl bonded to Ti on the surface. (See Fig. 2b.) HCl evolution(II) corresponds to the reaction between the Cl bonded to Ti and NH_x that are in 2NN relations, as shown in Fig. S1b. Lastly, both HCl evolution(III) and HCl evolution (IV) contain the reaction of Cl* and NH_x at the 1NN distance and distinguish whether the CN of NH_x is high (4, 5, and 6) or low (1, 2, and 3), respectively. (See Fig. S1c and d, respectively.).

The reaction energies are calculated from DFT calculations on initial and final configurations under diverse local environments counted in Table 1. We generate each configuration by placing various species on designated lattice sites in the 5-layer H-terminated TiN (111) slab, which is then fully relaxed. (See Sec. 2.2 for the detailed description of the base model.) When assigning TiCl₄ and NH_x species on lattice sites, we use relaxed structures in the gas phase or surface-adsorbed state to make a plausible initial guess. We confirm that the bonding topology of the relaxed structures is the same as intended. Fig. 3a shows the distribution of reaction energies for desorption, Cl dissociation, and HCl evolution as classified in Table 1. For the Cl₂ evolution, we simply use a single energy of 0.45 eV for every case because the reaction energies lie between 0.4 and 0.5 eV.

The rate constant in Eq. (5) requires the computation of activation barriers, which can be obtained by identifying the minimum energy path (MEP) via methods like NEB or string methods [51,54,55]. For desorption processes and Cl₂ evolutions, the reaction energies are always positive with the energies monotonically increasing along the reaction

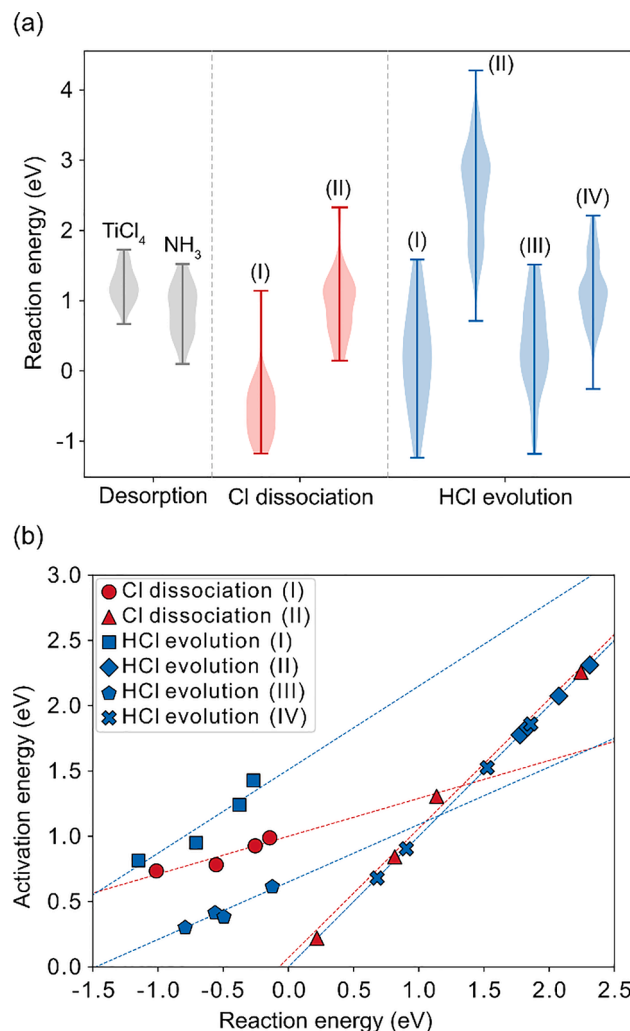


Fig. 3. (a) Violin plots of reaction energies for desorption, Cl dissociation, and HCl evolution. (b) Linear fitting of activation energies with respect to reaction energies for Cl dissociations and HCl evolutions.

pathway without transition states. As such, reaction energies are directly used as the activation energies. In Table 1, 849 events for the Cl dissociation and HCl evolution require activation energies from MEP, which is computationally too expensive. As an approximation, we infer activation energies from reaction energies, using the Bell-Evans-Polanyi

Table 1

Number of events and fitted parameters in the BEP relations for each reaction. In the HCl and Cl₂ evolutions, the neighboring relation between reacting molecules is indicated in the parentheses.

Reaction type	Subtype	Number of events	E_0 (eV)	α
Adsorption of precursors	TiCl ₄ (g) → TiCl ₄	1	-	-
	NH ₃ (g) → NH ₃	1	-	-
Desorption of precursors	TiCl ₄ → TiCl ₄ (g)	35	-	-
	NH ₃ → NH ₃ (g)	18	-	-
Cl dissociation	(I) TiCl ₄ → TiCl ₃ + Cl*	30	1.00	0.29
	(II) Cl → Cl*	103	0.07	0.99
HCl evolution	(I) TiCl ₄ + NH _x (1NN) → TiCl ₃ + NH _{x-1} + HCl(g)	44	1.51	0.64
	(II) Cl + NH _x (2NN) → NH _{x-1} + HCl(g)	345	0.00	1.00
	(III) Cl* + NH _x (1NN-high CN) → NH _{x-1} + HCl(g)	90	0.65	0.44
	(IV) Cl* + NH _x (1NN-low CN) → NH _{x-1} + HCl(g)	237	0.00	1.00
Cl ₂ evolution	Cl* + Cl* (2NN) → Cl ₂ (g)	287	-	-
Relaxation of NH _x and Cl	NH _x → NH _x	2	-	-
	Cl → Cl	1	-	-
Ti densification	Ti → Ti	1	-	-

(BEP) principle [56,57]. The BEP relation states that the activation energy varies linearly with the reaction enthalpy if the reactions belong to the same family. This relationship can be written as follows:

$$E^\ddagger = E_0 + \alpha \Delta E \quad (7)$$

where E^\ddagger is the activation energy, ΔE is the reaction enthalpy (reaction energy in the present work), and E_0 and α are fitting parameters. Thus, we sample four reactions from each distinct reaction family and calculate E^\ddagger by employ the CI-NEB method. E_0 and α are then fitted and all the other activation energies are calculated from the reaction energy and fitted parameters. Fig. 3b shows the fit to the BEP relation and the fitted E_0 and α are compiled in Table 1. For all the reactions with purely positive reaction energies, $E_0 = 0$ and $\alpha = 1$, which means that the transition state is missing along the reaction pathway and the (positive) reaction energy is equal to the activation energy, like in the desorption or Cl_2 evolution. Finally, we compute 902 reaction energies and activation barriers to construct the event table.

3. Results and discussions

3.1. KMC simulation of ALD process

The conditions for the present kMC simulation are adopted from typical experiments [19,26], and one ALD cycle consists of sequential steps of TiCl_4 dose (0.1 sec), purge (1.5 sec), NH_3 dose (1.0 sec), and purge (1.5 sec). In purge steps, the adsorption of precursors is switched off while other reactions are allowed to happen. The partial pressure is

set to 40 and 330 mTorr for TiCl_4 and NH_3 , respectively, and the process temperature is varied from 300 to 500 °C with the interval of 50 °C. The kMC simulation starts from the TiN (111) surface that is fully terminated with NH species. The lateral dimension of the simulation box is $30.04 \times 26.02 \text{ \AA}^2$ comprising 100 lattice sites in each layer. For the statistical average, five independent simulations are carried out under each condition with different random seeds.

Fig. 4a shows the thickness of deposited films as a function of the ALD cycle at various temperatures. The thickness is defined as the average height of the top occupied sites in the Ti sublattice with respect to the topmost Ti layer in the initial substrate. In Fig. 4a, the linear growth is observed at every temperature with the slope increasing with the deposition temperature. By computing the slope calculated with data points excluding initial cycles (1 ~ 3), one can obtain the growth per cycle (GPC), as shown in Fig. 4b together with previous experimental measurements [19,20,26,44,58]. We note that experimental films are always polycrystalline phases comprising (111) and (200) surfaces (see above) although no clear distinction was reported for the growth rate depending on the crystal orientation [19,44]. The large scatter of growth rate among experimental literature can be attributed to different process conditions such as working pressures [59]. It is seen that agreements between theory and experiment are good. In particular, the saturation behavior of GPC between 400 and 500 °C in Ref. [43] is well reproduced. In Fig. 4b, the growth rate saturates at 0.21 TiN layer per cycle and this value will be explained in the below based on the detailed growth mechanism. For the fully grown layers, the concentration of Ti (N) vacancies is 3% (1%) at 300 °C, which decreases to 1.1% (0.6%) at 400 °C. To check the dependence of the initial condition on the growth rate, we also perform the kMC simulation at 400 °C starting with the NH_2 -terminated surface and find that GPC converges to 0.47 Å/cycle, close to 0.49 Å/cycle in Fig. 4b.

In Fig. 4a, the slope changes slightly after 10 cycles at 300 °C. From the detailed analysis, it is found that relative populations of various surface species are stabilized after 8 cycles at 300 °C (see Fig. S3a). This transient behavior may have caused the slight change in the growth rate at 300 °C. In contrast, at 400 °C, the distribution of surface species is rapidly stabilized after 3 cycles (see Fig. S3b).

3.2. Growth mechanism

To understand the atomistic growth mechanism of the TiN-ALD process, we analyze the simulation data in more detail. Fig. 5a shows a representative mass-gain profile during one ALD cycle at 400 °C. (As far as we are aware, there is no experimental mass-profile measurements on TiN-ALD using $\text{TiCl}_4/\text{NH}_3$.) One can observe a sharp increase in mass at the beginning of the TiCl_4 dose due to heavy masses of Ti and Cl in comparison with N and H. During the TiCl_4 dose, the dominant species on the surface rapidly changes from NH_x to Cl, as can be seen in Fig. 5b (see the top of Fig. 5a for the instance of the snapshot). After the surface is saturated with Cl, no further reactions occur other than adsorption and desorption of TiCl_4 , which is indicative of the self-limiting behavior. To reveal more details of the process, we present in Fig. 5d the number of selected events for each event during kMC, which is averaged over the last 10 cycles. When adsorbed TiCl_4 molecules are attached to the surface in the form of $-\text{TiCl}_3$, 74% of them generate Cl^* , while the rest produced HCl gas molecules. Additional Cl^* species are created by breaking Ti-Cl bonds in $-\text{TiCl}_3$ on the surface. This is followed by HCl and Cl_2 gas molecules evolving from Cl^* . On the other hand, after the NH_3 dose, the dominant species on the surface changes from Cl to NH_x (see Fig. 5c). As the NH_3 molecule is relatively small, occupying only one lattice site, the steric effect is not significant. Instead, the self-limiting behavior during the NH_3 dose originates from the lack of available adsorption sites. The detailed reaction pathway can be understood by the frequency of reaction events in Fig. 5d. First, as the coverage of NH_3 increases, Cl^* sites above H become stabilized, and this leads to the Cl dissociation in existing TiCl_x groups. Then HCl gas molecules evolve

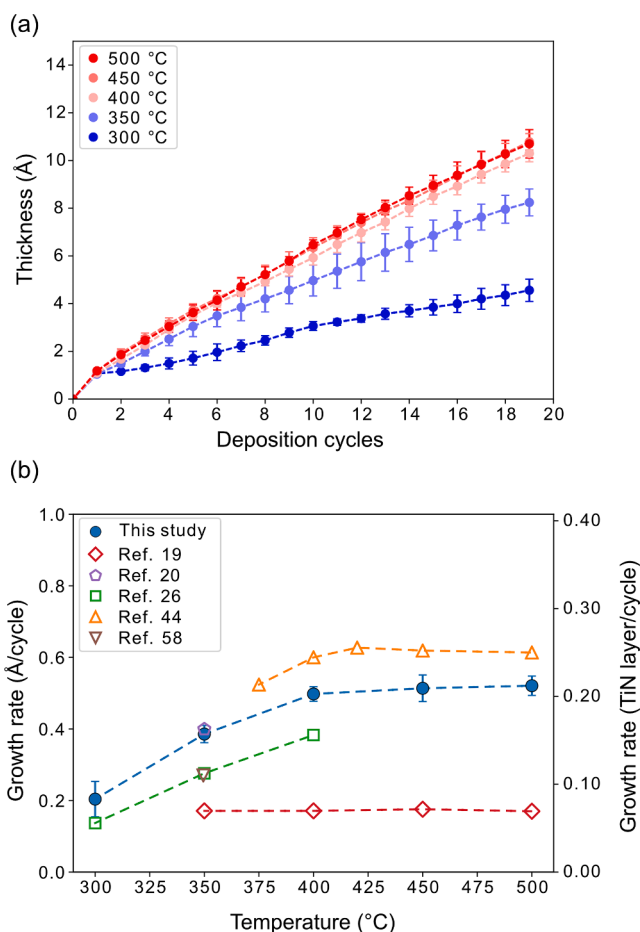


Fig. 4. (a) The thickness of deposited TiN layers with respect to the ALD cycle. The error bars indicate standard deviations among the five independent simulations. (b) The growth rate of TiN films at different process temperatures in comparison with experimental data.

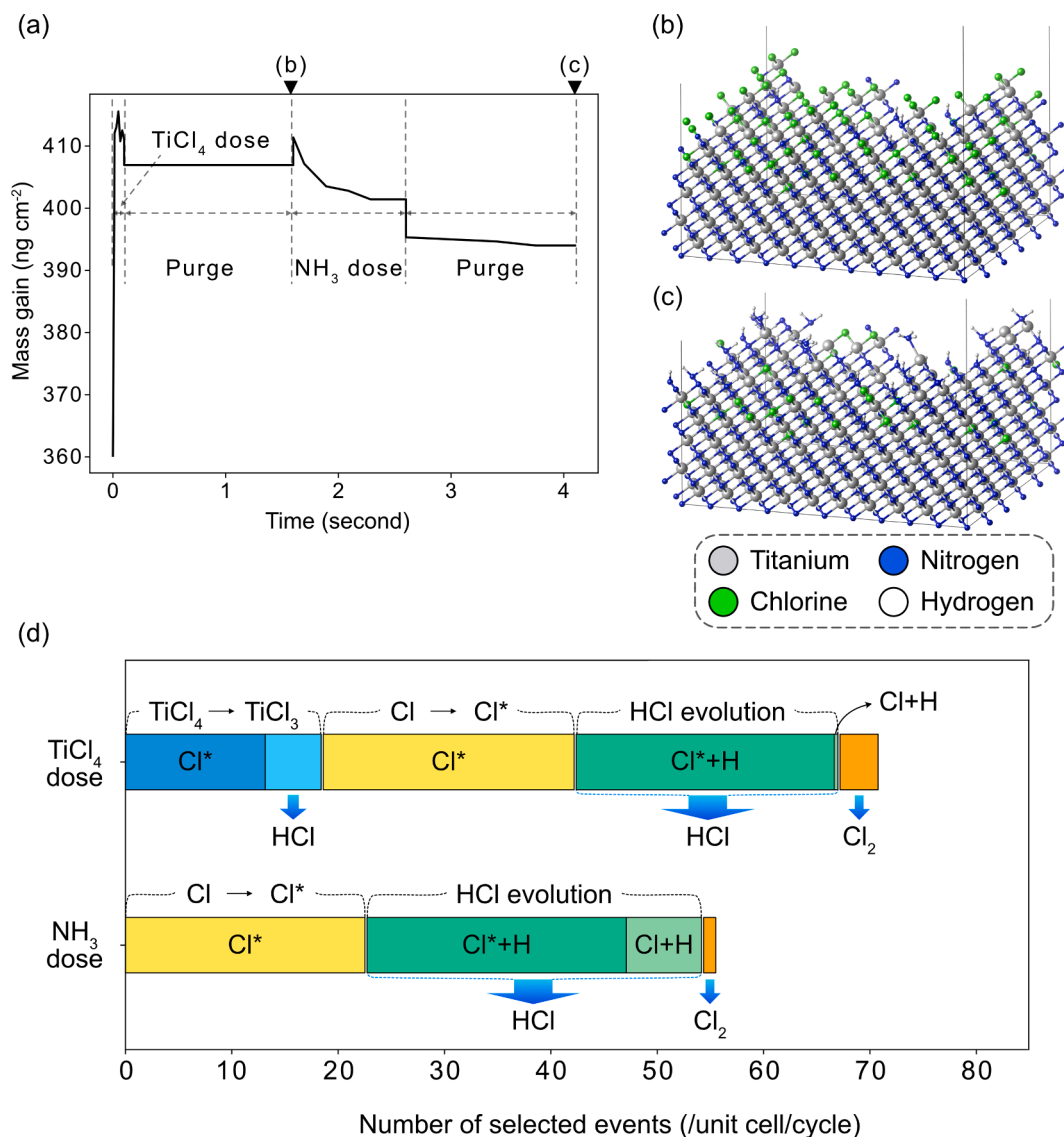


Fig. 5. (a) A representative mass gain profile during one ALD cycle at 400 °C. The simulation snapshots after TiCl_4 and NH_3 doses, taken at the instances at the top, are presented in (b) and (c), respectively. (d) The number of selected events for Cl dissociations and HCl/ Cl_2 evolutions during one ALD cycle, which is averaged over the last 10 cycles.

from reactions between H and Cl or Cl^* . A small amount of Cl_2 gas also evolves.

In Fig. 4b, the maximum GPC was found to be 0.2 TiN layer per cycle, which merits further explanation. Due to the steric hindrance among Cl atoms in $-\text{TiCl}_3$ species, the maximum coverage of Ti layer is 1/3 or 33%, which theoretically corresponds to the growth rate of 0.33 TiN layer per cycle. However, there exist Cl atoms on the surface that did not react in the previous cycles (see Fig. 5c), which constrain the maximum coverage of TiCl_3 groups well below the ideal value. This results in the saturated value of 0.2 TiN layer per cycle in Fig. 4b.

3.3. Cl contamination

As mentioned in the introduction, the Cl contamination is a major problem in the ALD process using TiCl_4 , which increases resistivity. In Fig. 6a, we plot the Cl concentration remnant in the deposited film with respect to the temperature, along with experimental results [20,26,60,61]. Although experimental data widely vary, the simulation results agree reasonably with the experiment, in particular those from Ref. [26] at low temperatures. The decrease of Cl impurities at high

temperatures is also well reproduced. However, the simulation results tend to overestimate the Cl concentration, and we infer that this quantitative difference is due to the unreacted Cl^* in the film. At high temperatures, more than 50% of residual Cl exists in the form of Cl^* , but since we do not strictly consider the diffusion of Cl^* , it may remain in an environment where there are few hydrogen atoms to react.

To check whether 20 cycles are statistically sufficient for Cl contamination, we additionally simulate TiN-ALD process up to 50 cycles at 300 and 500 °C. It is found that Cl concentration is slightly decreased from 17.8% to 15.2% at 300 °C and 6.2% to 5.3% at 500 °C. Thus the overall trend does not change significantly.

We find that Cl impurities can be classified into unreacted or dissociated Cl atoms (see Fig. 6b). The unreacted Cl remains in the N sublattice bonded to Ti, meaning that the Ti-Cl bond in the original precursor is intact. On the other hand, dissociated Cl atoms in the Ti sublattice did not evolve into HCl or Cl_2 gas molecules. The populations of the two types of Cl residues are shown as stacked bars in Fig. 6a. At 300 °C, unreacted Cl is the major source of Cl contamination, taking up 85%. This is due to strong Ti-Cl bonds that require high thermal energies for bond breaking. As the temperature increases, Ti-Cl bonds are more

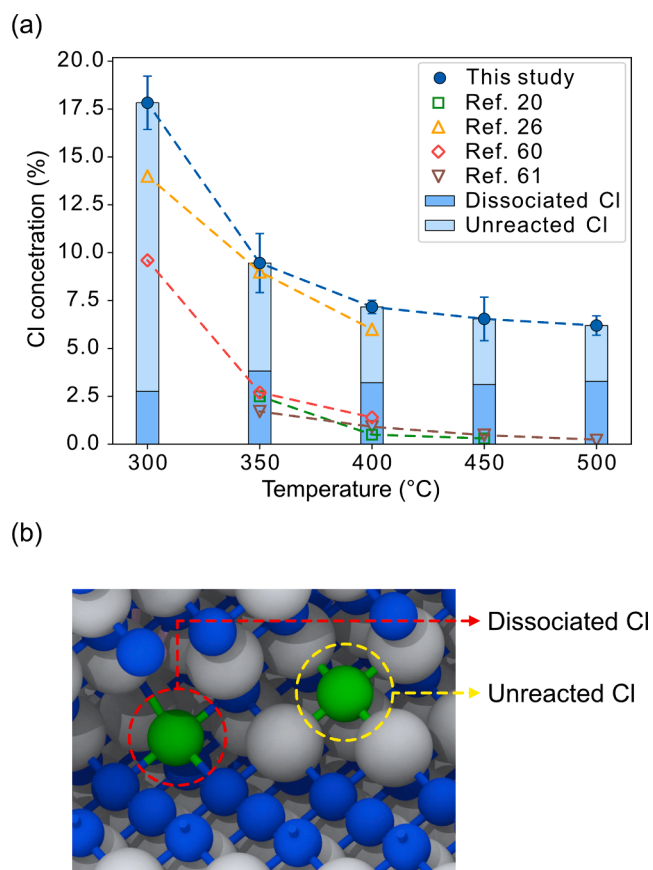


Fig. 6. (a) The Cl concentration remnant in the deposited film with respect to the temperature, along with experimental results. (b) Two types of Cl residues, dissociated or unreacted, that remain in the deposited film.

readily broken, which mainly contributes to the reduction of Cl residues. The analysis in the present and previous sections indicate that the generation of Cl* from the dissociation of Cl ligands from the precursor is a major limiting step in the ALD process employing TiCl_4 and NH_3 .

It is seen in Fig. 6a that the amounts of unreacted Cl change significantly as the temperature increases above 350 °C, which indicates crossover from one mechanism to another, although it is difficult to resolve full details. This transition in the growth mechanism may have caused large error bars for the growth rate in Fig. 4a.

Since remnant Cl contents are overestimated in comparison with experiment, the reaction mechanism of TiN-ALD from TiCl_4 and NH_3 is still not fully resolved, and there could be other reaction pathways for Cl_2 evolution that are missing in the present study. In passing, to examine whether the choice of k_0 in Eq. (5) can affect the result, we vary the parameter from 1 to 5 and 10, and the resulting Cl contamination decreased slightly from 7.2% to 7.0% and 7.1%, respectively.

4. Summary and conclusion

In summary, we carried out kMC simulations on the ALD process using TiCl_4 and NH_3 precursors. Based on the on-lattice model, we sorted out key chemical processes relevant for ALD such as adsorption/dissociation of precursors, generation of surface Cl atoms, and evolution of HCl and Cl_2 gas molecules, considering local environments affecting the energy of chemical species. The reaction energies were explicitly calculated at the DFT level while the activation barriers were linearly fitted to sampled cases among distinct reaction families, following the BEP principle. The resulting kMC produced the growth rate and the amount of Cl residues that are in reasonable agreements with experiment, implying that key chemical reactions are well captured by the

present model. However, the overestimation of Cl impurities at high temperatures still raises the need for additional reaction path for Cl removal, which should be identified in future study. A detailed growth pathway was revealed and underscores the critical role of surface Cl atoms that are dissociated from TiCl_4 in the ALD process by generating HCl gas. In conclusion, by revealing the key atomistic processes in the TiN-ALD process, the present work would help mitigate impurities and increase conductivities of TiN thin films.

CRediT authorship contribution statement

Sangtae Kim: Software, Investigation, Formal analysis, Writing – original draft. **Hyungmin An:** Software, Investigation, Writing – original draft. **Sangmin Oh:** Formal analysis, Investigation. **Jisu Jung:** Formal analysis, Software. **Byungjo Kim:** Conceptualization, Funding acquisition. **Sang Ki Nam:** Conceptualization, Funding acquisition. **Seungwu Han:** Conceptualization, Supervision, Writing – review & editing.

Declaration of Competing Interest

The authors declare that they have no known competing financial interests or personal relationships that could have appeared to influence the work reported in this paper.

Data Availability.

The data that support the plots within this paper and other findings of this study are available from the corresponding author upon reasonable request.

Acknowledgements

This work was supported by Mechatronics Research, Samsung Electronics Co., Ltd. and the computations were carried out at the Korea Institute of Science and Technology Information (KISTI) super-computing center (KSC-2021-CRE-0476).

Appendix A. Supplementary material

Supplementary data to this article can be found online at <https://doi.org/10.1016/j.commat.2022.111620>.

References

- [1] H. O. Pierson, Handbook of Refractory Carbides and Nitrides: Properties, Characteristics, Processing and Applications, Noyes, Westwood, NJ, 1996.
- [2] T. Echtermeyer, H.D.B. Gottlob, T. Wahlbrink, T. Mollenhauer, M. Schmidt, J. K. Efavi, M.C. Lemme, H. Kurz, Investigation of MOS capacitors and SOI-MOSFETs with epitaxial gadolinium oxide (Gd_2O_3) and titanium nitride (TiN) electrodes, Solid-State Electron. 51 (2007) 617–621, <https://doi.org/10.1016/j.sse.2007.02.008>.
- [3] C. Fenouillet-Beranger, S. Denorme, P. Perreau, C. Buj, O. Faynot, F. Andrieu, L. Tosti, S. Barnola, T. Salvétat, X. Garros, M. Cassé, F. Allain, N. Loubet, L. Pham-Nguyen, E. Deloffre, M. Gros-Jean, R. Beneyton, C. Laviron, M. Marin, C. Leyris, S. Haendler, F. Leverd, P. Gouraud, P. Scheiblin, L. Clement, R. Pantel, S. Deleonibus, T. Skotnicki, FDSOI devices with thin BOX and ground plane integration for 32nm node and below, Solid-State Electron. 53 (2009) 730–734, <https://doi.org/10.1016/j.sse.2009.02.009>.
- [4] C.J. Brennan, C.M. Neumann, S.A. Vitale, Comparison of gate dielectric plasma damage from plasma-enhanced atomic layer deposited and magnetron sputtered TiN metal gates, J. Appl. Phys. 118 (2015), 045307, <https://doi.org/10.1063/1.4927517>.
- [5] M. Moriyama, T. Kawazoe, M. Tanaka, M. Murakami, Correlation between microstructure and barrier properties of TiN thin films used Cu interconnects, Thin Solid Films. 416 (2002) 136–144, [https://doi.org/10.1016/S0040-6090\(02\)00602-8](https://doi.org/10.1016/S0040-6090(02)00602-8).
- [6] J.Y. Kim, S. Seo, D.Y. Kim, H. Jeon, Y. Kim, Remote plasma enhanced atomic layer deposition of TiN thin films using metalorganic precursor, J. Vac. Sci. Technol. Vac. Surf. Films. 22 (2004) 8–12, <https://doi.org/10.1116/1.1624285>.
- [7] H.C.M. Knoops, L. Baggetto, E. Langereis, M.C.M. van de Sanden, J.H. Klootwijk, F. Roozeboom, R.A.H. Niessen, P.H.L. Notten, W.M.M. Kessels, Deposition of TiN

- and TaN by Remote Plasma ALD for Cu and Li Diffusion Barrier Applications, *J. Electrochem. Soc.* 155 (2008) G287, <https://doi.org/10.1149/1.2988651>.
- [8] J.S. Chawla, X.Y. Zhang, D. Gall, Epitaxial TiN(001) wetting layer for growth of thin single-crystal Cu(001), *J. Appl. Phys.* 110 (2011), 043714, <https://doi.org/10.1063/1.3624773>.
- [9] L. Djomeni, T. Mourier, S. Minoret, S. Fadloun, F. Piallat, S. Burgess, A. Price, Y. Zhou, C. Jones, D. Mathiot, S. Maitrejean, Study of low temperature MOCVD deposition of TiN barrier layer for copper diffusion in high aspect ratio through silicon vias, *Microelectron. Eng.* 120 (2014) 127–132, <https://doi.org/10.1016/j.mee.2013.11.010>.
- [10] J. Speulmanns, A.M. Kia, K. Kühnel, S. Bönhardt, W. Weinreich, Surface-Dependent Performance of Ultrathin TiN Films as an Electrically Conducting Li Diffusion Barrier for Li-Ion-Based Devices, *ACS Appl. Mater. Interfaces.* 12 (2020) 39252–39260, <https://doi.org/10.1021/acsmi.0c10950>.
- [11] R.D. Chavan, M.M. Tavakoli, D. Prochowiec, P. Yadav, S.S. Lote, S.P. Bhoite, A. Nimbalkar, C.K. Hong, Atomic Layer Deposition of an Effective Interface Layer of TiN for Efficient and Hysteresis-Free Mesoscopic Perovskite Solar Cells, *ACS Appl. Mater. Interfaces.* 12 (2020) 8098–8106, <https://doi.org/10.1021/acsmi.9b18082>.
- [12] A. Sherman, Growth and Properties of Low Pressure Chemical-Vapor-Deposited TiN for Ultra Large Scale Integration, *Jpn. J. Appl. Phys.* 30 (1991) 3553–3557, <https://doi.org/10.1143/JJAP.30.3553>.
- [13] E.O. Travis, R.W. Fiordalice, Manufacturing aspects of low pressure chemical-vapor-deposited TiN barrier layers, *Thin Solid Films.* 236 (1993) 325–329, [https://doi.org/10.1016/0040-6090\(93\)90690-Q](https://doi.org/10.1016/0040-6090(93)90690-Q).
- [14] S.R. Kurtz, R.G. Gordon, Chemical vapor deposition of titanium nitride at low temperatures, *Thin Solid Films.* 140 (1986) 277–290, [https://doi.org/10.1016/0040-6090\(86\)90271-3](https://doi.org/10.1016/0040-6090(86)90271-3).
- [15] M.J. Buiting, A.H. Reader, Influence of Impurities and Microstructure on the Resistivity of LPCVD Titanium Nitride Films, in: T.M. Besmann, B.M. Gallois (Eds.), *Chemical Vapor Deposition of Refractory Metals and Ceramics*, Materias Research Society, Pittsburgh, PA, 1990, pp. 199–204.
- [16] A. Sherman, Growth and Properties of LPCVD Titanium Nitride as a Diffusion Barrier for Silicon Device Technology, *J. Electrochem. Soc.* 137 (6) (1990) 1892–1897, <https://doi.org/10.1149/1.2086826>.
- [17] J.Y. Kim, G.H. Choi, Y.D. Kim, Y. Kim, H. Jeon, Comparison of TiN Films Deposited Using Tetrakisdimethylamino-titanium and Tetrakisdiethylamino-titanium by the Atomic Layer Deposition Method, *Jpn. J. Appl. Phys.* 42 (2003) 4245–4248, <https://doi.org/10.1143/JJAP.42.4245>.
- [18] J. Kim, H. Hong, S. Ghosh, K.-Y. Oh, C. Lee, Physical Properties of Highly Conformal TiN Thin Films Grown by Atomic Layer Deposition, *Jpn. J. Appl. Phys.* 42 (2003) 1375–1379, <https://doi.org/10.1143/JJAP.42.1375>.
- [19] C.H. Ahn, S.G. Cho, H.J. Lee, K.H. Park, S.H. Jeong, Characteristics of TiN thin films grown by ALD using TiCl₄ and NH₃, *Met. Mater. Int.* 7 (2001) 621–625, <https://doi.org/10.1007/BF03179261>.
- [20] H. Jeon, J.-W. Lee, Y.-D. Kim, D.-S. Kim, K.-S. Yi, Study on the characteristics of TiN thin film deposited by the atomic layer chemical vapor deposition method, *J. Vac. Sci. Technol. Vac. Surf. Films.* 18 (2000) 1595–1598, <https://doi.org/10.1116/1.582391>.
- [21] K.-E. Elers, J. Winkler, K. Weeks, S. Marcus, TiCl₄ as a Precursor in the TiN Deposition by ALD and PEALD, *J. Electrochem. Soc.* 152 (8) (2005) G589–G593, <https://doi.org/10.1149/1.1938108>.
- [22] M. Ritala, M. Leskelä, E. Rauhala, P. Haussalo, Atomic Layer Epitaxy Growth of TiN Thin Films, *J. Electrochem. Soc.* 142 (8) (1995) 2731–2737, <https://doi.org/10.1149/1.2050083>.
- [23] M. Ritala, T. Asikainen, M. Leskelä, J. Jokinen, R. Lappalainen, M. Utriainen, L. Niinistö, E. Ristolainen, Effects of intermediate zinc pulses on properties of TiN and NbN films deposited by atomic layer epitaxy, *Appl. Surf. Sci.* 120 (1997) 199–212, [https://doi.org/10.1016/S0169-4332\(97\)00387-5](https://doi.org/10.1016/S0169-4332(97)00387-5).
- [24] M. Juppo, A. Rahtu, M. Ritala, In Situ Mass Spectrometry Study on Surface Reactions in Atomic Layer Deposition of TiN and Ti(Al)N Thin Films, *Chem. Mater.* 14 (2002) 281–287, <https://doi.org/10.1021/cm011150r>.
- [25] M. Bosund, A. Aierken, J. Tiilikainen, T. Hakkarainen, H. Lipsanen, Passivation of GaAs surface by atomic-layer-deposited titanium nitride, *Appl. Surf. Sci.* 254 (2008) 5385–5389, <https://doi.org/10.1016/j.apsusc.2008.02.070>.
- [26] H.J. Lee, J.H. Hwang, J.-Y. Park, S.W. Lee, Alternative Surface Reaction Route in the Atomic Layer Deposition of Titanium Nitride Thin Films for Electrode Applications, *ACS Appl. Electron. Mater.* 3 (2021) 999–1005, <https://doi.org/10.1021/acsaem.0c01079>.
- [27] M.J. Buiting, A.F. Otterloo, A.H. Montree, Kinetic Aspects of the LPCVD of Titanium Nitride from Titanium Tetrachloride and Ammonia, *J. Electrochem. Soc.* 138 (2) (1991) 500–505, <https://doi.org/10.1149/1.2085618>.
- [28] H. Tiznado, F. Zaera, Surface Chemistry in the Atomic Layer Deposition of TiN Films from TiCl₄ and Ammonia, *J. Phys. Chem. B.* 110 (2006) 13491–13498, <https://doi.org/10.1021/jp062019f>.
- [29] M. Andersen, C. Panosetti, K. Reuter, A Practical Guide to Surface Kinetic Monte Carlo Simulations, *Front. Chem.* 7 (2019) 202, <https://doi.org/10.3389/fchem.2019.00202>.
- [30] N. Cheimarios, D. To, G. Kokkoris, G. Memos, A.G. Boudouvis, Monte Carlo and Kinetic Monte Carlo Models for Deposition Processes: A Review of Recent Works, *Front. Phys.* 9 (2021), 631918, <https://doi.org/10.3389/fphy.2021.631918>.
- [31] G. Mazaleyrat, A. Estève, L. Jeloaiça, M. Djafari-Rouhani, A methodology for the kinetic Monte Carlo simulation of alumina atomic layer deposition onto silicon, *Comput. Mater. Sci.* 33 (2005) 74–82, <https://doi.org/10.1016/j.commatsci.2004.12.069>.
- [32] A. Dkhissi, A. Estève, C. Mastail, S. Olivier, G. Mazaleyrat, L. Jeloaiça, M., Djafari Rouhani, Multiscale Modeling of the Atomic Layer Deposition of HfO₂ Thin Film Grown on Silicon: How to Deal with a Kinetic Monte Carlo Procedure, *J. Chem. Theory Comput.* 4 (2008) 1915–1927, <https://doi.org/10.1021/ct8001249>.
- [33] M. Shirazi, S.D. Elliott, Atomistic kinetic Monte Carlo study of atomic layer deposition derived from density functional theory, *J. Comput. Chem.* 35 (2014) 244–259, <https://doi.org/10.1002/jcc.23491>.
- [34] T. Weckman, M. Shirazi, S.D. Elliott, K. Laasonen, Kinetic Monte Carlo Study of the Atomic Layer Deposition of Zinc Oxide, *J. Phys. Chem. C.* 122 (2018) 27044–27058, <https://doi.org/10.1021/acs.jpcc.8b06909>.
- [35] S.H. Lee, H. Park, H. Kim, M.-H. Huang, A study of MgF₂ thin film growth in the atomic layer deposition process by multi-scale simulations, *Comput. Mater. Sci.* 191 (2021), 110327, <https://doi.org/10.1016/j.commatsci.2021.110327>.
- [36] Y. Mochizuki, Y. Okamoto, A. Ishitani, K. Hirose, T. Takada, On the Reaction Scheme for Ti/TiN Chemical Vapor Deposition (CVD) Process Using TiCl₄, *Jpn. J. Appl. Phys.* 34 (1995) L326–L329, <https://doi.org/10.1143/JJAP.34.L326>.
- [37] A.G. Baboul, H.B. Schlegel, Structures and Energetics of Some Potential Intermediates in Titanium Nitride Chemical Vapor Deposition: TiCl_m(NH₂)_n, TiCl_m(NH₂)_nNH, and TiCl_m(NH₂)_nN, *An ab Initio Molecular Orbital Study*, *J. Phys. Chem. B.* 102 (1998) 5152–5157, <https://doi.org/10.1021/jp9810668>.
- [38] T. Tanaka, T. Nakajima, K. Yamashita, Density functional study on the adsorption and surface reactions on SiO₂ in TiN-CVD using TiCl₄ and NH₃, *Thin Solid Films.* 409 (2002) 51–57, [https://doi.org/10.1016/S0040-6090\(02\)00103-7](https://doi.org/10.1016/S0040-6090(02)00103-7).
- [39] W. Choi, S. Lee, D.-H. Han, H.T. Lim, H. Park, G.-D. Lee, Reaction mechanisms of chlorine reduction on hydroxylated alumina in titanium nitride growth: First principles study, *Appl. Surf. Sci.* 550 (2021), 149391, <https://doi.org/10.1016/j.apsusc.2021.149391>.
- [40] K. Toyoura, T. Fujii, N. Hatada, D. Han, T. Uda, Carrier-Carrier Interaction in Proton-Conducting Perovskites: Carrier Blocking vs Trap-Site Filling, *J. Phys. Chem. C.* 123 (2019) 26823–26830, <https://doi.org/10.1021/acs.jpcc.9b08199>.
- [41] A.B. Bortz, M.H. Kalos, J.L. Lebowitz, A New Algorithm for Monte Carlo Simulation of Ising Spin Systems, *J. Comput. Phys.* 17 (1975) 10–18, [https://doi.org/10.1016/0021-9991\(75\)90060-1](https://doi.org/10.1016/0021-9991(75)90060-1).
- [42] H. Eyring, The Activated Complex in Chemical Reactions, *J. Chem. Phys.* 3 (1935) 107–115, <https://doi.org/10.1063/1.1749604>.
- [43] K. Reuter, D. Frenkel, M. Scheffler, The Steady State of Heterogeneous Catalysis, Studied by First-Principles Statistical Mechanics, *Phys. Rev. Lett.* 93 (2004), 116105, <https://doi.org/10.1103/PhysRevLett.93.116105>.
- [44] J. Kim, H. Hong, K. Oh, C. Lee, Properties including step coverage of TiN thin films prepared by atomic layer deposition, *Appl. Surf. Sci.* 210 (2003) 231–239, [https://doi.org/10.1016/S0169-4332\(03\)00158-2](https://doi.org/10.1016/S0169-4332(03)00158-2).
- [45] G. Kresse, J. Furthmüller, Efficiency of ab-initio total energy calculations for metals and semiconductors using a plane-wave basis set, *Comput. Mater. Sci.* 6 (1996) 15–50, [https://doi.org/10.1016/0927-0256\(96\)00008-0](https://doi.org/10.1016/0927-0256(96)00008-0).
- [46] G. Kresse, J. Furthmüller, Efficient iterative schemes for ab initio total-energy calculations using a plane-wave basis set, *Phys. Rev. B.* 54 (1996) 11169–11186, <https://doi.org/10.1103/PhysRevB.54.11169>.
- [47] P.E. Blöchl, Projector augmented-wave method, *Phys. Rev. B.* 50 (1994) 17953–17979, <https://doi.org/10.1103/PhysRevB.50.17953>.
- [48] J.P. Perdew, K. Burke, M. Ernzerhof, Generalized Gradient Approximation Made Simple, *Phys. Rev. Lett.* 77 (1996) 3865–3868, <https://doi.org/10.1103/PhysRevLett.77.3865>.
- [49] S. Grimme, J. Antony, S. Ehrlich, H. Krieg, A consistent and accurate ab initio parametrization of density functional dispersion correction (DFT-D) for the 94 elements H-Pu, *J. Chem. Phys.* 132 (2010), 154104, <https://doi.org/10.1063/1.3382344>.
- [50] G. Henkelman, B.P. Uberuaga, H. Jónsson, A climbing image nudged elastic band method for finding saddle points and minimum energy paths, *J. Chem. Phys.* 113 (2000) 9901–9904, <https://doi.org/10.1063/1.1329672>.
- [51] G. Henkelman, H. Jónsson, Improved tangent estimate in the nudged elastic band method for finding minimum energy paths and saddle points, *J. Chem. Phys.* 113 (2000) 9978–9985, <https://doi.org/10.1063/1.1323224>.
- [52] S. Smidstrup, A. Pedersen, K. Stokbro, H. Jónsson, Improved initial guess for minimum energy path calculations, *J. Chem. Phys.* 140 (2014), 214106, <https://doi.org/10.1063/1.4878664>.
- [53] A. Hjorth Larsen, J. Jørgen Mortensen, J. Blomqvist, I.E. Castelli, R. Christensen, M. Dulak, J. Friis, M.N. Groves, B. Hammer, C. Hargus, E.D. Hermes, P.C. Jennings, P. Bjerre Jensen, J. Kermod, J.R. Kitchin, E. Leonhard Kolsbjerg, J. Kubal, K. Kaasbjerg, S. Lysgaard, J. Bergmann Maronsson, T. Maxson, T. Olsen, L. Pastewka, A. Peterson, C. Rostgaard, J. Schiøtz, O. Schütt, M. Strange, K. S. Thygesen, T. Vegge, L. Vilhelmsen, M. Walter, Z. Zeng, K.W. Jacobsen, The atomic simulation environment—a Python library for working with atoms, *J. Phys. Condens. Matter.* 29 (2017), 273002, <https://doi.org/10.1088/1361-648X/aa680e>.
- [54] B.J. Berne, G. Ciccotti, D.F. Coker, *Classical and Quantum Dynamics in Condensed Phase Simulations*, World Scientific, 1998.
- [55] W. E, W. Ren, E. Vanden-Eijnden, String method for the study of rare events, *Phys. Rev. B.* 66 (2002) 052301, <https://doi.org/10.1103/PhysRevB.66.052301>.
- [56] R.P. Bell, The theory of reactions involving proton transfers, *R. Soc.* 154 (1936) 414, <https://doi.org/10.1098/rspa.1936.0060>.
- [57] M.G. Evans, M. Polanyi, INERTIA AND DRIVING FORCE OF CHEMICAL REACTIONS, *Trans. Faraday Soc.* 34 (1938) 11, <https://doi.org/10.1039/TF9383400011>.
- [58] A. Satta, A. Vantomme, J. Schuhmacher, C.M. Whelan, V. Sutcliffe, K. Maex, Initial growth mechanism of atomic layer deposited TiN, *Appl. Phys. Lett.* 84 (2004) 4571–4573, <https://doi.org/10.1063/1.1760217>.

- [59] J. Aarik, A. Aidla, A. Kasikov, H. Mändar, R. Rammula, V. Sammelseg, Influence of carrier gas pressure and flow rate on atomic layer deposition of HfO₂ and ZrO₂ thin films, *Appl. Surf. Sci.* 252 (2006) 5723–5734, <https://doi.org/10.1016/j.apsusc.2005.07.067>.
- [60] K.-E. Elers, V. Saanila, P.J. Soininen, W.-M. Li, J.T. Kostamo, S. Haukka, J. Juhanaja, W.F.A. Besling, Diffusion Barrier Deposition on a Copper Surface by Atomic Layer Deposition, *Chem. Vap. Depos.* 8 (2002) 149, [https://doi.org/10.1002/1521-3862\(20020704\)8:4<149::AID-CVDE149>3.0.CO;2-F](https://doi.org/10.1002/1521-3862(20020704)8:4<149::AID-CVDE149>3.0.CO;2-F).
- [61] J. Meersschaut, M. Käyhkö, H.P. Lenka, T. Witters, Q. Zhao, A. Vantomme, W. Vandervorst, RBS and PIXE analysis of chlorine contamination in ALD-Grown TiN films on silicon, *AIP Conference Proceedings* 1525 (2013) 190–194, <https://doi.org/10.1063/1.4802317>.